European Polymer Journal 196 (2023) 112324

Contents lists available at ScienceDirect

European Polymer Journal

journal homepage: www.elsevier.com/locate/europolj

Reversible bond formation via sulfur free reversible addition fragmentation in photo-3D printing

Zhongyuan Wan, Lee Wai Hin, Ataulla Shegiwal, David Haddleton

Department of Chemistry, University of Warwick, Coventry CV4 7AL, United Kingdom

A B S T R A C T

An addition-fragmentation monomer (AFM) has been used as a crosslinker in photopolymerization-based 3D printer resins in order to try and reduce shrinkage due to polymerisation. This results in reversible network formation via photo crosslinking with reversible covalent bond formation to effect mechanical performance. The 3D printing conditions were optimized with regards to print quality, print speed, etc. The AFM was synthesized via catalytic chain transfer polymerization (CCTP) and characterized using NMR and size exclusion chromatography (SEC). The incorporation of the AFM as a crosslinker allows for rapid reversible covalent bond formation during network formation in 3D photopolymerization printing resulting in a reduction in both polymerisation shrinkage and stress higher molecular weight crosslinkers lead to less shrinkage and reversible bond formation to less stress build up. Curing was monitored via photo-rheology and Fourier Transform Infrared Spectroscopy (FT-IR). At lower contents of AFM, the mechanical properties (strength and Young's modulus) are improved without compromising material properties, printing conditions and curing time. At higher AFM content, the kinetic analysis of the photopolymerization reaction shows a reduced final conversion of the vinylic bonds along with a delay of the gel point. The thermal and mechanical properties were evaluated with incorporation of different concentrations of AFM added to the resin formulations.

1. Introduction

There has been significant developments of photolithographic 3D printing for use in additive manufacturing. Photo-polymerization in general has been utilized in numerous applications including coatings [1], adhesives [2,3], inks [4,5], printing plates [6,7], optical wave guides [8] and microelectronics [9,10]. Photocuring is used in many different and diverse applications including acrylic dental restoration materials [11–13] and fabrication of 3D objects using a range of 3D printers and interestingly these processes, although seemingly very different, share many chemical aspects. 3D printing has attained considerable traction for the fabrication of objects in a layer-by-layer process and allows the acquisition of highly personalized design, high efficiency for production of small quantities of parts, and ease of fabrication of objects with complicated geometric structures. [14,15] Computer aided design (CAD) software is utilized to assist in the formation, manipulation, analysis, and optimization of 3D printed designs. [12,16] Each layer is bonded to the previous layer by either thermally, chemically, or mechanically, resulting in a replica of the original 3D CAD data, Fig. 1. Technologies have been developed, including stereolithography (SLA), digital light processing (DLP), fused filament modelling (FDM), liquid crystal display (LCD), selective laser sintering (SLS), multi jet fusion (MJF) etc. Stereolithography [17], LCD and DLP 3D printing [18], based on the UV-curing of photopolymer resins, are considered to have superior printing resolution together with high efficiency [19].

In SLA 3D printing a laser scans and cures the photo-polymerizable resin point by point whilst in DLP and LCD systems the UV light cures an entire layer of the resin at the same time with a single exposure, initiating free-radical polymerisation which results in crosslinked networks with non-reversible "permanent" covalent bonds. [1] SLA systems usually result in higher resolution and accuracy of the resulting 3D printed parts. DLP 3D printing has a distinctive advantage on the high printing speed which has resulted in exploration as an avenue for mass manufacturing. [20].

Resins utilized for photopolymerization crosslinking usually comprise of mixtures of mono functional monomers, difunctional vinyl monomers, crosslinkers, photo-initiators, dyes, and often fillers. The most widely utilized monomers are acrylates and methacrylates which are susceptible to polymerisation shrinkage. Shrinkage can lead to internal stress build up during the polymerization/crosslinking, resulting in a reduction in volume of the printed object during polymerization. This "shrinkage stress" can cause significant problems with regards material performance: for example, in dentistry, shrinkage of composite resin fillings upon hardening can cause the restoration to fail or even

This paper is part of a special issue in honor of Prof. Nikos Hadjichristidis to celebrate his contributions to the polymer science field and to mark his significant and valubale advice and mentoring.

E-mail address: d.m.haddleton@warwick.ac.uk (D. Haddleton).

https://doi.org/10.1016/j.eurpolymj.2023.112324
Received 19 June 2023; Received in revised form 20 July 2023; Accepted 23 July 2023
Available online 25 July 2023

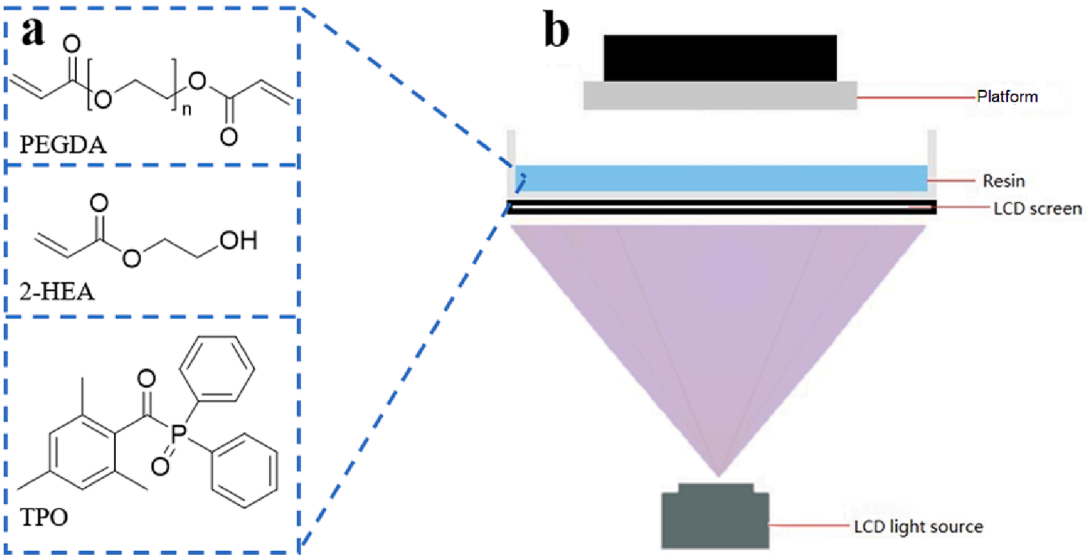

Fig. 1. a) Components used in photoinduced resin and composites used in this work. b) Schematic of 3D liquid–crystal display (LCD) printer working principle.

more dramatically [11,21].

There have been several studies that have addressed this issue focusing on reducing shrinkage stress and strain by both Boyer and Bowman. [22–26] An interesting application of a reversible addition fragmentation transfer (RAFT) process is the use of so called addition fragmentation monomers (AFM's) used for the reduction of stress in dental resins as reported in a series of elegant patents by 3 M [27–34]. Here the authors applied cobalt mediated catalytic chain transfer polymerisation (CCTP) to prepare dimethacrylic crosslinkers containing an internal carbon–carbon double bond which acts as a site for RAFT during radical propagation. It is also noted that they used a simplified version of the cobalt(II) catalyst, cobalt(II) bisdimethylglyoxime, avoiding the use of bridging BF_2 groups making catalyst synthesis trivial and as the reactions are carried out in the absence of acids hydrolysis is not a major issue. These AFM's were used to give reversible crosslinking during irradiation (radial formation) which is able to relieve stress accumulated through curing [35].

Approaches to alleviate this rigid network structure to allow for stress relaxation includes the use of covalent adaptable networks (CAN). [36] Covalent adaptable networks (CAN) offer a mechanism for stress relaxation [37,38]. This can lead to a significant reduction in stress relaxation by monomers containing an addition-fragmentation (AF) chain transfer moiety which has found commercial success in dental resins. [39] We hypothesized that a similar functional crosslinking

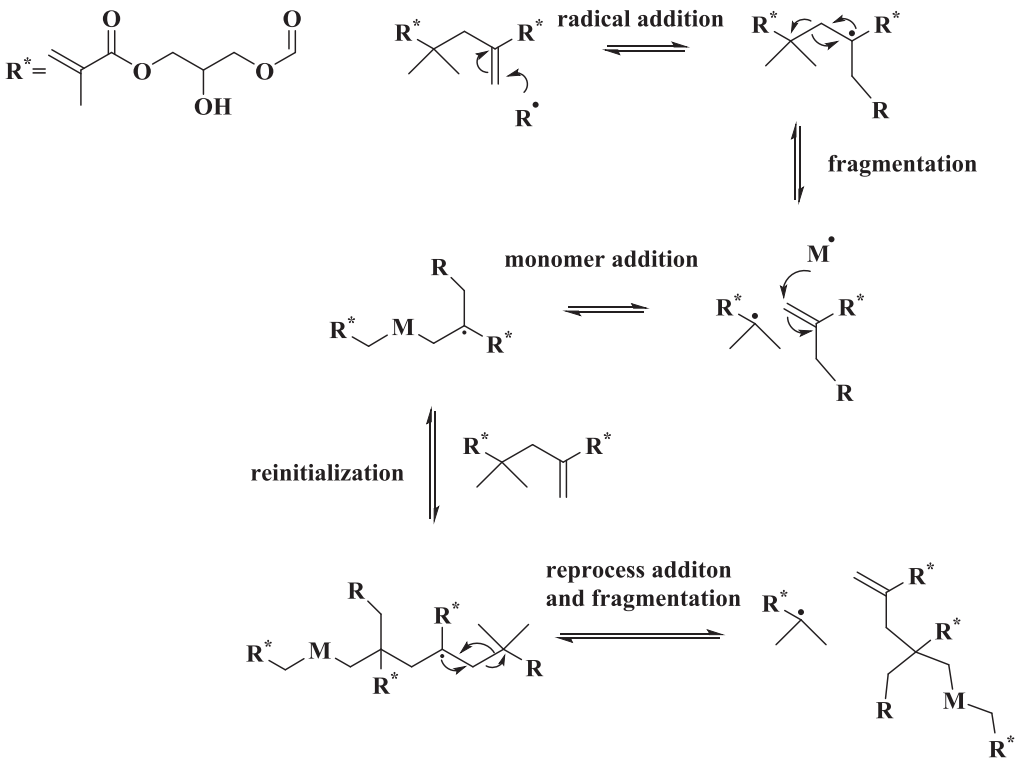

Scheme 1. Mechanism for the AFM addition-fragmentation process. The radical can further initiate polymerization or multiple addition-fragmentation steps to give a polymer that has a methacrylate terminated radical [35].

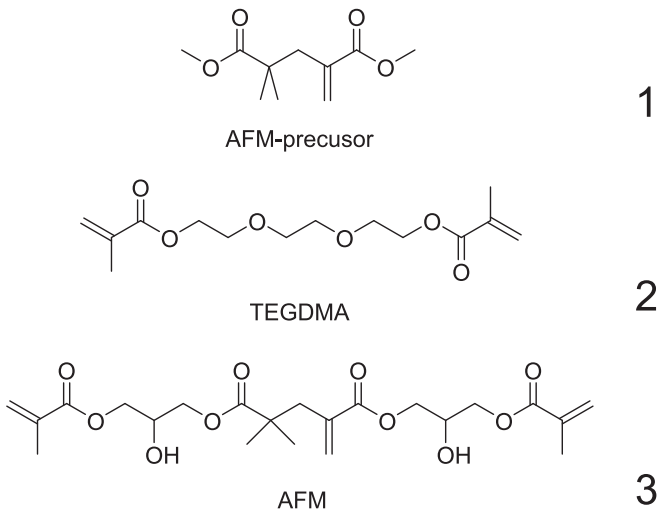

Fig. 2. Structure of AFM-precursor (**1, MMA$_2$**), Addition Fragmentation Monomers (AFM) (**3**) and Triethylene glycol dimethacrylate (TEGDMA) (**2**).

monomer could be used to give similar improvements in mechanical performance in photopolymerization-based 3D printing. This type of AF chain transfer monomer made by cobalt mediated CCTP [40,41,35] The AFMs are derived from methacrylic acid dimers as synthesized via the base hydrolysis of Co(II) mediated CCTP of methyl methacrylate (MMA) at relatively high catalyst levels and have two terminal methacrylate groups with a chemically different internal vinyl bond with a β-quaternary carbon center susceptible to undergoing reversible addition fragmentation and transfer (RAFT) in a methacrylate radical polymerization [42–46]. It is noted that this moiety retards the rate of polymerization due to a prolonged dormant radical state. The dimethacrylates readily participate in network formation by copolymerization with other multi and mono-functional methacrylates, or acrylates as with other dimethacrylate crosslinkers integrating into the network. [35] This current work describes the use of these AFMs as an additive to a 3D printing resin formulation in order to study the influence of the concentration of the AFM on photopolymerization kinetics and shrinkage stress in 3D printing.

Crosslinkers which contain an AFM participate in the reaction following an associative mechanism which can lead to stress relaxation, Scheme 1 [47,48]. In the presence of radicals, the propagating polymer chain can add to the internal double bond, undergo fragmentation to regenerate an active radical, which allows for re-initiation (RAFT, Scheme 1) [35,39]. The reversible formation and breaking of a covalent bond during the network formation is repeated continuously until all radicals terminate. This process has been reported to reduce shrinkage stresses during the photopolymerization in dental resins [49].

2. Results and discussion

2.1. Synthesis of the AFM, 3

Catalytic chain transfer polymerization (CCTP) of methyl methacrylate (MMA) using relatively high amounts of catalyst led to product with a high dimer content (**1**) with low amounts of trimer, tetramer, etc and high amounts of residual MMA. The dimer, **1**, was isolated by vacuum distillation and hydrolysed with sodium hydroxide to methacrylic acid dimer. AFM **3** was prepared by reaction of the methacrylic acid dimer with glycidyl methacrylate via ring opening catalyzed by triphenylantimony at 100 °C with subsequent addition of triphenylphosphine to give the product as a clear pale yellow viscous liquid following a modified procedure from the patent literature [58,59] The structure of the AFM and AFM-precursor were confirmed by ^{1}H NMR, Scheme 2, (Fig. 2). The AFM was added in different amounts to a standardized in-house printing formulation composed of 2-HEA and PEGDA-250 premixed in a weight ratio 100:50 with TPO at 0.5 wt% as a photoinitiator.

2.2. Optimization of the 3D printing conditions

Acrylic and methacrylic based monomers extensively utilized in photo-3D printing are susceptible to stress and shrinkages upon curing. We based our selection on monomers derived from acrylic monomers as they have a higher rate of propagation and react faster than methacrylic counterparts which results in significantly faster curing time between each layer of prints.

PEG-diacrylate offers high resolution and enables printing of fine details as it is particularly sensitive to UV-Light which is important for achieving accurate and precise 3D models. Furthermore, PEG-diacrylate resins often have low viscosity, meaning they flow easily. This property allows for better levelling and spreading of the resin during the printing process, resulting in smoother and more consistent prints.

HEA is a hydroxy functional acrylate that is often used as a reactive diluent and monomer in conjunction with PEG-diacrylate for formulation of resins. Reduction in shrinkage is important for maintaining dimensional accuracy and minimizing potential warping or distortion. HEA can also improve the mechanical properties of the printed objects, such as flexibility and impact resistance. By blending HEA with PEG-diacrylate, the resulting resins can have enhanced toughness and durability.

After deciding the monomer compositions in the resin formulation, the printing parameters were optimized. Different printer parameters lead to significant changes in the quality and mechanical performance of the printed part and were adjusted to optimize the printing conditions by changing the light intensity resulting in changes in resolution. The Nova Bene Mono 4 printer (LCD type) is reported to give 45 um resolution working at $\lambda = 405$ nm with commercial UV resin formulations at approximately 3.5 mW cm^{-2} light intensity. Due to the increasing viscosity of the resin at higher concentrations of **3**, it is necessary to optimize the printing conditions such that complete parts were printed within the entire range of AFM concentration used (0 to 16 wt%), Table 1. The resin in the resin tank was changed after each print run as the colour of the resin changed and the material properties of the printed parts showed slight differences if this was not carried out. Between each print run the printer was left idle for at least 30 mins to allow the light intensity to return to the original value as measured by an "Optical Power and Energy Meter Console (Thorlabs PM400)". It was observed during the work that increasing the concentration of **3** up to 8 wt% increased the physical and thermal properties, Fig. 6 and Fig. 7 whilst at concentrations > 8 wt%, the properties of the resins were compromised, Table 1 (see Table 2).

Prior to testing the printed parts, the conversion was determined by FTIR spectroscopy using the C = O stretching band at 1720 cm^{-1} and C = C stretching at 1635 cm^{-1} (Fig. 3) by comparing the intensity of 1635 cm^{-1} of the C = C stretching band, normalized at 1720 cm^{-1} of the C = O stretching band. The disappearance of C = C in the parts following 3D printing suggested high conversions in all cases. Moreover, all the spectra of all the printed parts closely overlapped (Figure SI 17 and Table SI 2). This indicated the deviations in the conversion and chemical compositions among the printed parts with different AFM content were miniscule, and eliminated the possible artefacts due to the variation in double bond conversions in later mechanical testing.

2.3. Tensile test results

A series of formulations were prepared which varied the relative amounts of 2-HEA, PEGDA$_{250}$ and **3**, Table SI 1.

The Young's modulus of the printed samples with between 0 and 8 wt% **3** were measured on the 5th day after printing after being stored under the same storage conditions (covered with aluminum foil and left

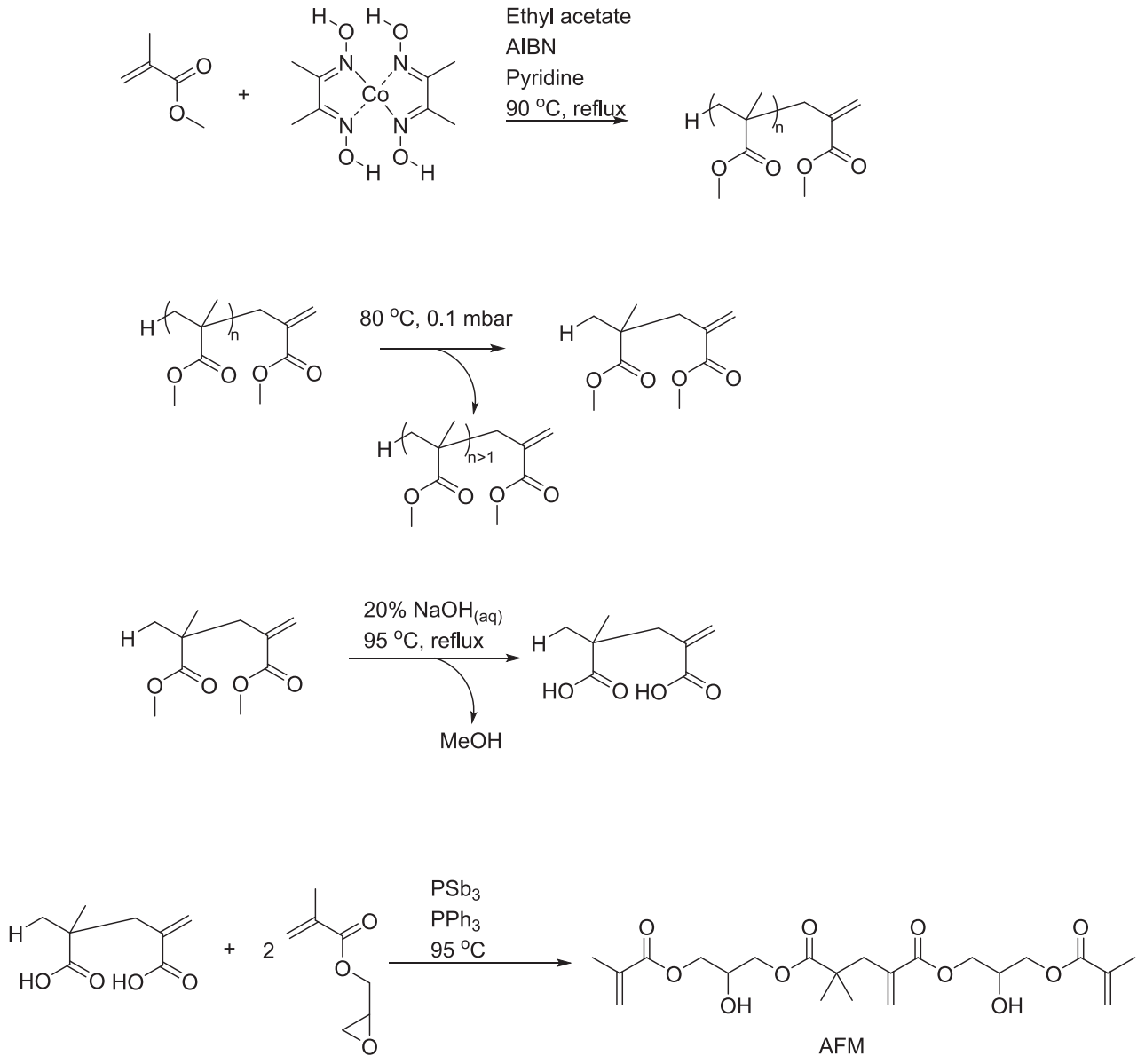

Scheme 2.

Table 1
Optimization conditions for the Nova Bene Mono 4 (LCD type) of in-house resin (weight ratio of 2-HEA: PEGDA 250: TPO = 100:50:0.75), with 0 wt%, 0.5 wt%, 1 wt%, 1.5 wt%, 2.0 wt%, 3 wt%, 4 wt%, 5 wt%, 6 wt%, 8 wt% and 16 wt% concentrations of AFM.

	Bottom layer	Normal layer
Layer thickness/ (um)	50	50
Exposure time/ (second)	90	25
Cure time/ (second)	10	10

at ambient temperature for 5 days) in order to minimize the effect of the time lag and storage history (Fig. 4). The Young's modulus of the printed parts increased with an increase in the concentration of **3** from 0.5 wt% to 4 wt% the Young's modulus increases by 24%, and with 8 wt% to 46%. For the mixed resin (PEGDA/2-HEA) the elastic modulus is affected by both temperature and ambient UV light, the samples were divided into 2 comparison groups, one covered with aluminum foil to prevent exposure to stray light and the second exposed to normal ambient sunlight to simulate more closely real working 3D printed parts.

Reduced amounts of **3** results in an increase in the tensile strength, Young's modulus, elongation at break and maximum stress, Fig. 5 and Fig. 6. The Young's modulus of the formulation with 8 wt% **3** were deemed to have the optimum properties immediately after printing with the same result detected with the samples covered with foil or exposed to sunlight, Fig. 5 a) and b). However, the Young's modulus of the samples with 8 and 6 wt% **3** showed a rapid decline over the five days. This decrease in the Young's modulus over time (Figure SI 7) remains speculative but it was expected to be related to the internal structure caused by AFM in excess, instead of environmental conditions because all samples were stored under identical environments and the decay was not observed in other cases. However, the enhancements in the mechanical properties by the AFM were still significant when a steady value reached a constant value after 5 days. At 2 wt% loading there is an effective impact on Young's modulus compared to 4 wt% and no added **3**. With 2 wt% there is a relatively high Young's modulus over the 5 days and this was considered to be the optimum formulation.

The stress at break point of various formulations containing **3** exhibited a similar trend to the changes of Young's modulus, the maximum stress declined over 5 days Fig. 6 a) and c). The 2 wt% **3**

Table 2
Stress and Young's modulus of 2-HEA/PEGDA$_{250}$ resin (5th day), Anycubic resin (5th day) and Photocentric resin (42nd day) resin of formulation with 0 wt% and 2 wt % AFM.

Proportion of **3**	0 wt%		2 wt%		Max Stress increasing (%)	Young's modulus increasing (%)
Characteristics	Max Stress (MPa)	Young's modulus (MPa)	Max Stress (MPa)	Young's modulus (MPa)		
2-HEA/PEGDA$_{250}$ resin (5th day)	5	18	9	25	80%	39%
Anycubic resin (5th day)	45	945	59	1176	31%	24%
Photocentric resin (42nd day)	43	428	49	712	14%	66%

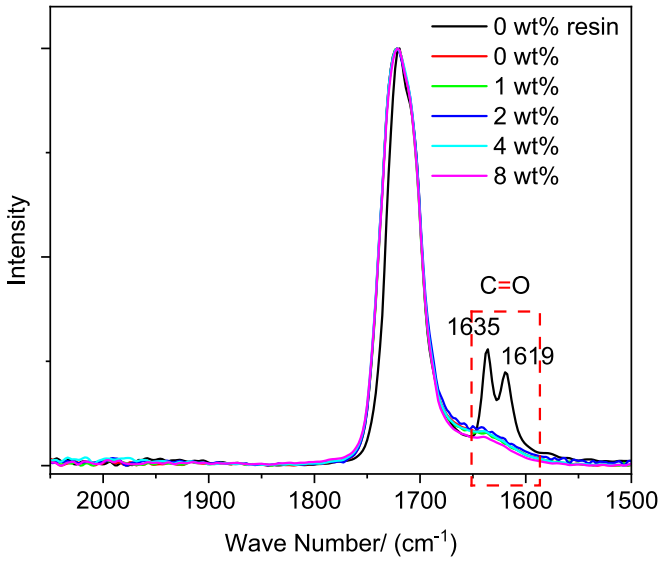

Fig. 3. FT-IR spectrum of objects after and before printed. 0 wt% resin (black), 0 wt% (red), 1 wt% (green), 2 wt% (blue), 4 wt%(cyan), 8 wt% (magenta). (For interpretation of the references to colour in this figure legend, the reader is referred to the web version of this article.)

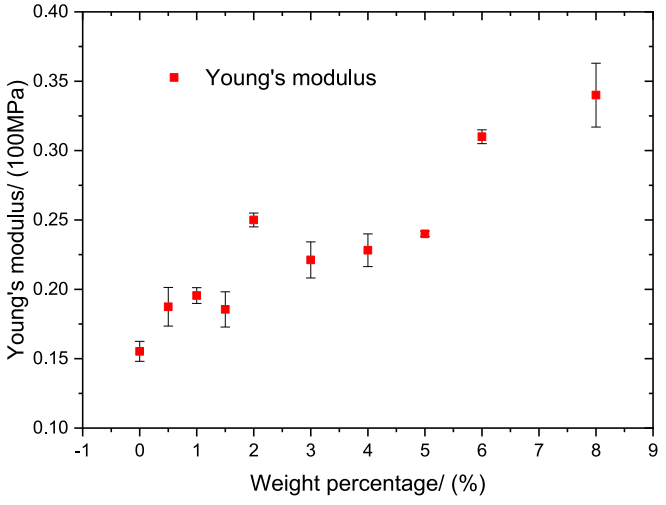

Fig. 4. Average Young's modulus of different wt% of **3** added to the in-house resin (2-HEA/PEGDA$_{250}$) as measured on the 5th day following printing and stored covered with aluminum foil.

formulation shows significant changes after 5 days, the maximum stress exceeds 8 wt% when covered in aluminum. This was also seen in samples left under normal sunlight. Formulations with 6 and 8 wt% **3** showed faster decreases when covered with aluminum than under sunlight. Thus, while the formulation with 4 wt% **3** does not show an obvious difference between the two different conditions this indicates that not all the **3** crosslinks into the network at 4 wt% during curing.

The strain also changed over 5 days, Fig. 6 b) and d), under the two different conditions. The strain of all formulations decreased over five days with 2 wt% **3** reaching the highest maximum strain. The maximum stress correlates well with the amount of **3**, while the critical stress first increases with the **3** content, and then decreases after 2 wt%, corresponding to a change in the strength and the modulus of the AFM content. The results indicate an optimum **3** proportion of 2 wt%, with Young's modulus, stress and strain enhanced by 52.6%, 82.4% and 16.1%. Thus, we decided that the optimum formulation contained 2 wt % **3**. The shrinkage is lower, 20%, and the stress can be improved significantly after five days.

The AFM was subsequently added to two different commercial resins, Anycubic (*Translucent UV Resin Green*), and Photocentric (*Daylight Magna Resin Black*). These two commercial resins are both curable under UV at $\lambda = 405$ nm, allowing comparison with the in-house resins. The Young's modulus of the commercial resins with added **3** showed no significant changes being left for 5 days, Fig. 7. The value recorded for the unadulterated Anycubic commercial resin fluctuates from 25% to 41%, and the increasing value of the Youngs modulus for the formulation containing 4 wt% AFM, from 50% to 56%. Taking into account the stability of the material, comparing these three proportions, 2 wt% of **3** again shows the highest stability and resistance to deformation.

A further comparison group was prepared using the Photocentric resin (*Daylight Magna Resin Black*), the stiffest material used in this study. These were subjected to a 42-day test with a measurement taken every 7 days. Three observations were made, firstly, all materials properties showed a downward overall trend under both incident light conditions, Fig. 8. Secondly, the stress and elastic modulus showed a higher value for the samples left exposed to normal ambient light than when covered in foil indicating some post printing cure occurring. Thirdly, at 2 wt% **3** there is a higher average stress and elastic modulus than in the pure commercial resin. The change on maximum stress and Young's modulus decreases to 15% and 2.5%. compared with the pure commercial resin with the average Young's modulus increasing over 60% and the average stress increasing by 14%.

2.4. Thermal properties

In order to assess any potential negative effects on the properties of the bulk material with the inclusion of **3**, the glass transition temperature (T_g) was measured by DSC, Fig. 9. From this the apparent T_g of the AFM and the base resin were 296 °C and 294 °C respectively.

Samples showed only one thermal degradation step between 350 °C and 430 °C corresponding to the decomposition of the PEGDA network (Fig. 10). Increasing the amount of **3** showed a negligible effect.

2.5. Photorheology

It was expected that the presence of addition fragmentation would

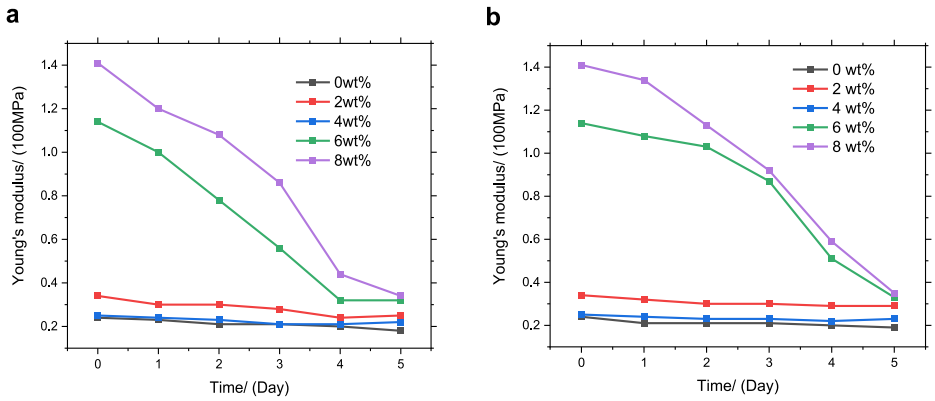

Fig. 5. Young's modulus as a function of time with the addition of 0, 2, 4, 6 and 8 wt% **3** with a 2-HEA/PEGDA$_{250}$ resin. a) covered by aluminum foil and b) left under normal ambient sunlight.

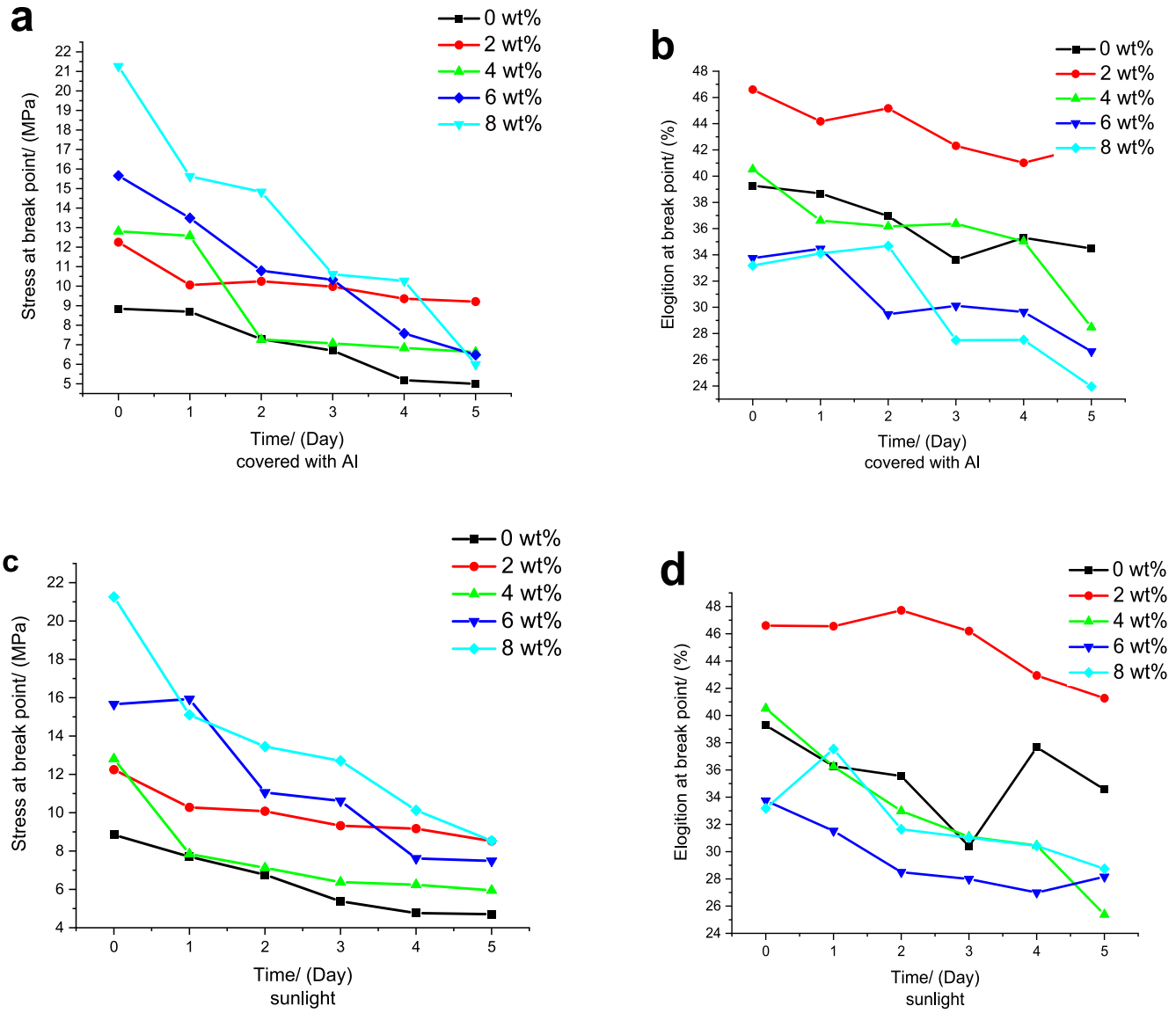

Fig. 6. Effect of addition of **3** (0, 2, 4, 6, 8 wt%) with a 2-HEA/PEGDA$_{250}$ resin on stress and strain a) and b) samples covered with aluminum foil; c), d) sample left in a normal sunlight environment.

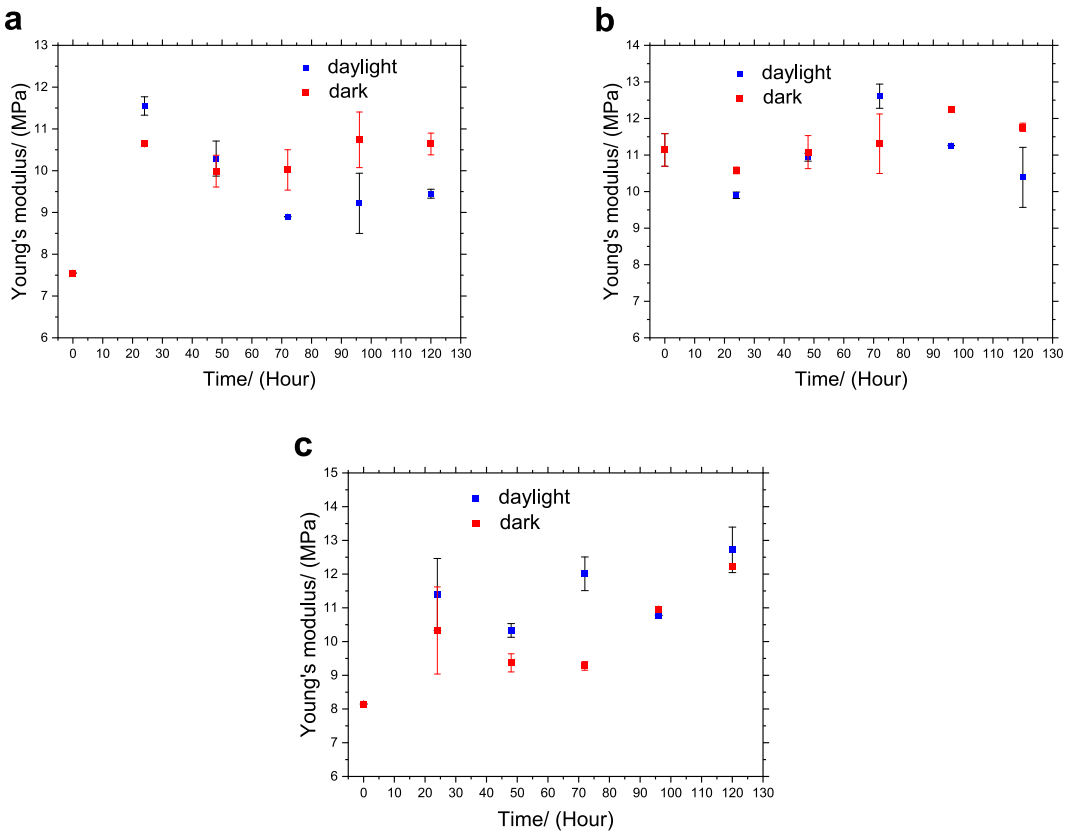

Fig. 7. Young's modulus measured over 5 days (a) Anycubic resin, (b) Anycubic resin with 2 wt% **3** and (c) Anycubic resin with 4 wt% **3**.

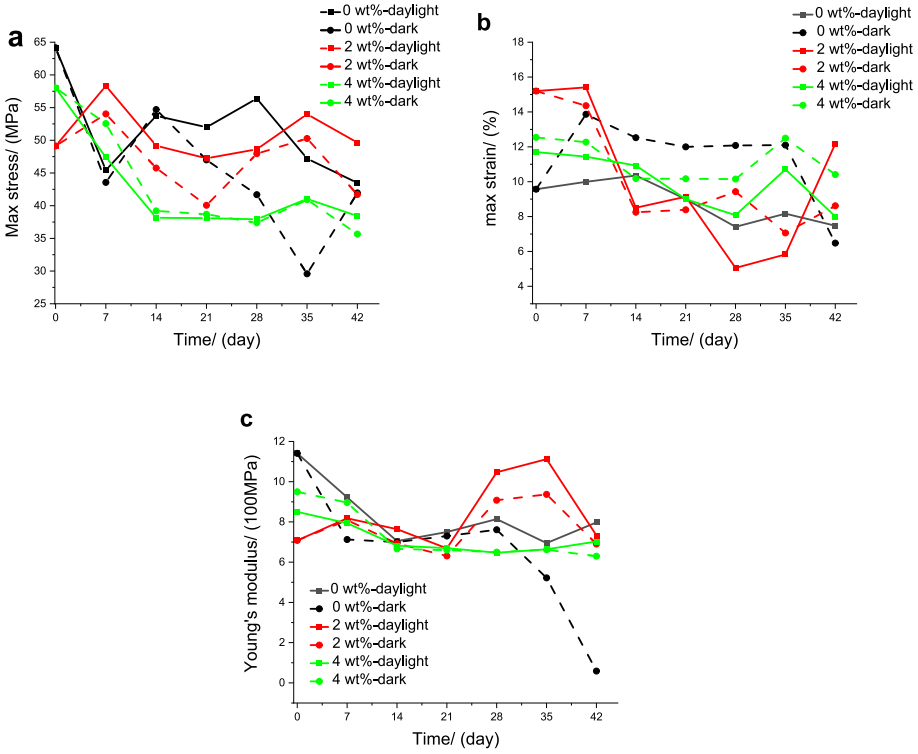

Fig. 8. Mechanical properties of (*Daylight Magna Resin Black*) Photocentric commercial resin measured over 42 days a) stress, b) strain and c) Young's modulus. (Solid line: sample left under normal ambient sunlight conditions; Dashed line: sample covered with aluminum).

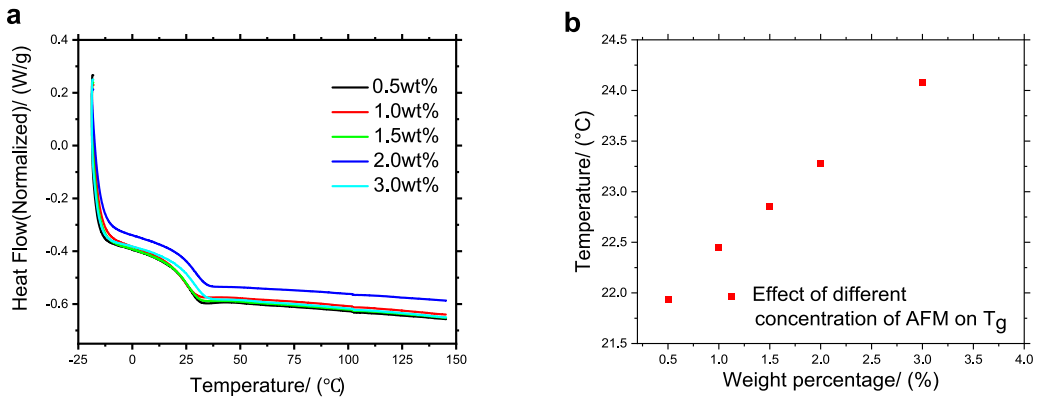

Fig. 9. (a) dsc traces and b) onset of T_g for 2-HEA/$PEGDA_{250}$ resin with 0 wt%, 0.5 wt%, 1.0 wt%, 1.5 wt%, 2.0 wt% and 3.0 wt% added AFM.

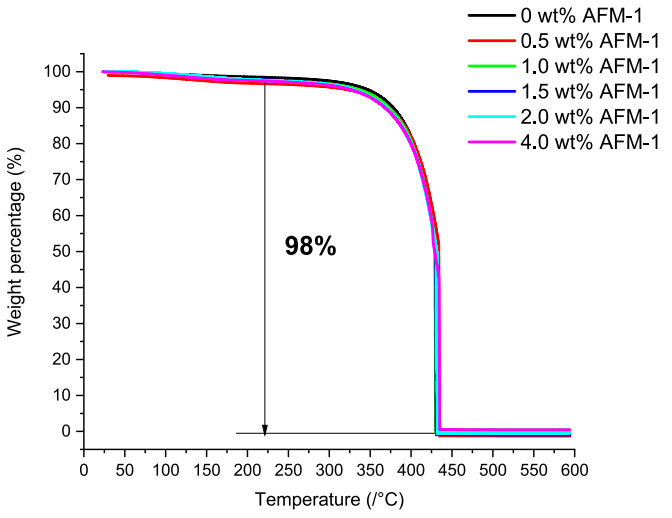

Fig. 10. Thermal decomposition (TGA) of formulations with 0, 0.5, 1.0, 1.5, 2.0 and 4.0 wt% of **3** in 2-HEA/$PEGDA_{250}$ resin.

reduce the time taken to reach the gel point. [50] Photorheology was used with the initial thickness of the formulation set as 400 μm and varied during the experiment so as to prevent detachment and slippage caused by polymerization shrinkage. [51,52] The gel point was determined at $\tan_\delta = G''/G' = 1$ [53,54,55] The gel point of the in-house resin with respect to 0, 2, 4 wt% **3** to the reactions monomers mixture at varied light intensity, Fig. 11, Table 3 (Fig. 12 and Table 4).

The gel point was delayed with increasing amounts of **3** at all light intensities (Fig. 13). This is attributed to the chain transfer activity of the β-quaternary vinyl group in **3**. It has previously been reported that the addition of chain transfer agent (CTA) in the polymerization of multifunctional (meth)acrylates could suppress the degree of crosslinking thus hindering or retarding gelation [56]. In terms of polymerization kinetics, chain transfer event shorten the instantaneous chain length and thus the average number of branching points per molecule; therefore, macroscopic gelation occurs at a higher conversion than that in the absence of CTA [57].

To investigate the effect on the gel point of the internal vinyl group in the AFM, TEGDMA with the same weight percentage was used as a control as TEGDMA does not have internal double bonds and thus cannot undergo addition fragmentation. The intensity of the light was maintained at 1L (4.88 m $\frac{W}{cm^2}$). Benchmark experiments were performed with TEGDMA as the dimethacrylate crosslinker without the reactive AFM vinyl group in varied concentration. As the total concentration of crosslinker TEGDMA increased the gel point crossover remained similar irrespective of the concentration of TEGDMA with respect to AFM. In the presence of the AFM a slight increase in, gel point was initially observed from 1 wt% compared with TEGDA, and more significant increase in gel point was observed at 16 wt%, which is attributed to the longer gel point time 169 s. This highlights the importance of the bi-substituted vinyl group in the AFM has involved in the forming-breaking process leading to a change in the gel point.

Due to the limitation of the geometry in the rheometer detachment from the parallel plates should occur with polymerization-induced shrinkage and thus conventional axial force measurement controlled by constant gap distance was not practical. The experiment was changed so as to apply a constant axial force with a varied gap distance over time. Since the shrinkage stress was allowed to be relieved by this dimensional change over time, as opposed to accumulating throughout the experiment, it was not necessary to consider any time dependence. In order to illustrate the effect of **3** on the shrinkage stress, the apparent shrinkage stress was estimated according to ***Equation 1***, where σ_s is shrinkage stress, G' is the experimentally measured storage modulus and γ(t) is the instantaneous strain calculated from the fitting in gap distance, with the assumption that the storage modulus by oscillation test was isotropic and represented the homogeneous bulk material. Fig. 13 **a and b** shows the calculated shrinkage stress as a function of time with an increasing concentration of **3** and TEGDMA respectively, Fig. 13 c). At 8 wt% **3**, there was a significant reduction in the cumulative shrinkage stress from 1.55 to 1.13 MPa, a 27% reduction, suggesting that part of the shrinkage stress was dissipated during the experiment. The time-dependence results also highlight the effect of the **3** on the evolution of the shrinkage stress.

In the absence of **3**, the shrinkage stress built up rapidly to a maximum of 33 kPa in < 1 min. Increasing the concentration of **3** resulted in the evolution of shrinkage stress being delayed and the maximum suppressed. At 8 wt% the maximum shrinkage stress was 2.9 kPa at 650 s. Moreover, the evolution of the shrinkage stress spanned over 10 min at higher concentrations of **3**, thus this prevented stress development beyond the limit of the crosslinked system instantaneously and caused deformation and mechanical damage.

$$\sigma_s = G' \times \gamma(t) \quad \text{(Equation 4)}$$

While the chemical mechanism(s) for the suppression and delay in the shrinkage stress could not be deduced from rheology, it was postulated that the inclusion of **3** reduced the shrinkage stress via two pathways. Firstly, **3** retards polymerization rate by lowering the effective transient concentration of propagating radical. Increasing concentration of **3** results in more radicals being deactivated temporarily, and a slower rate of polymerization thus stress development. Secondly, the β-quaternary vinyl group serves as a reversible crosslink point. Shrinkage stress develops when the volumetric shrinkage is limited, in this case by crosslinking. Once the polymeric radical is released via the fragmentation, the accumulated stress is able to relax via segmental motions, but

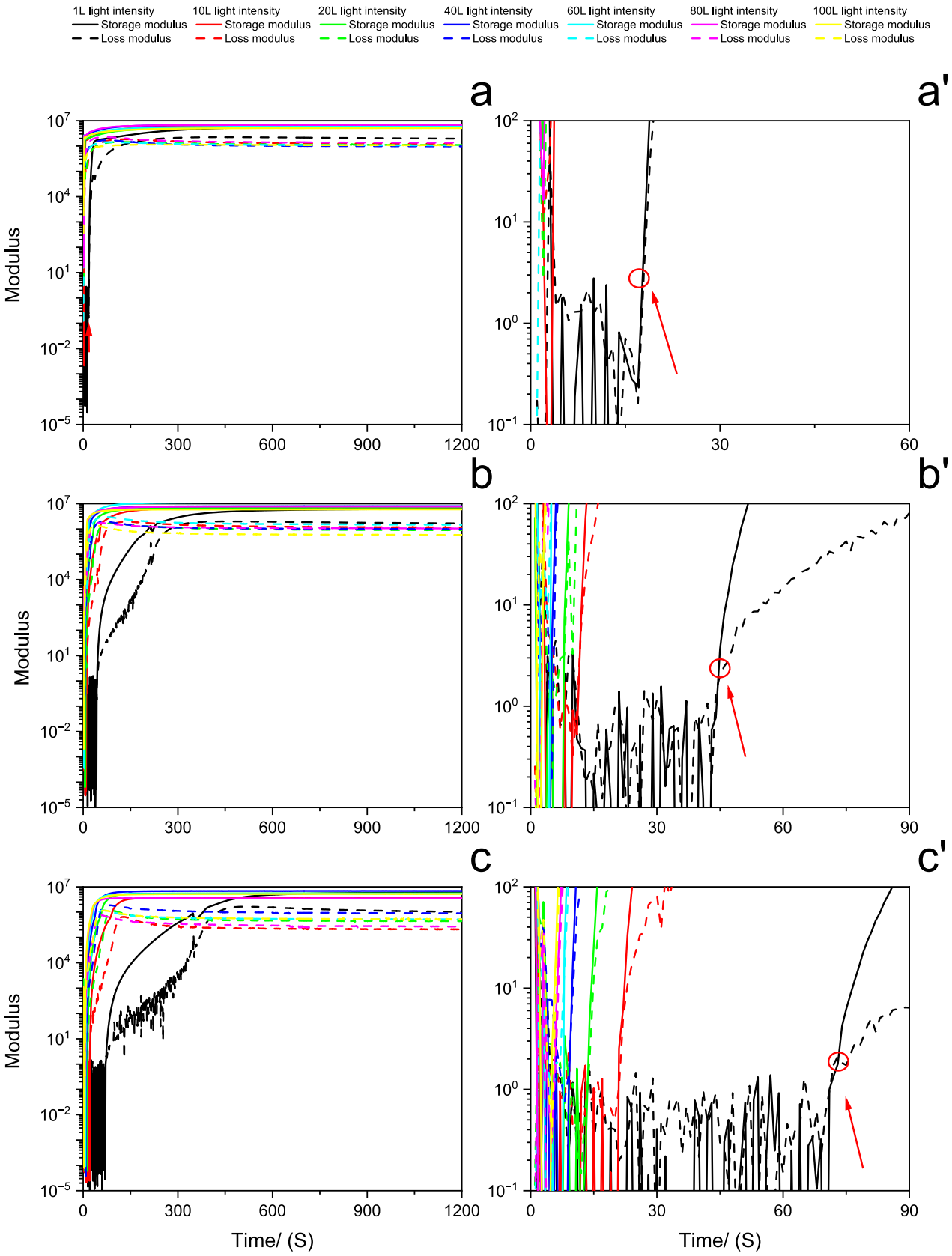

Fig. 11. Light intensity: 1L (black),10L (red), 20L (green), 40L (blue), 60L (cyan), 80L (magenta),100L (yellow). a), b), c) Evolution of the storage and loss modulus at 0, 2, 4 wt% of **3** within the 2-HEA/PEGDA$_{250}$ resin by increasing the light-intensity. a`), b`), c`) The zoom-in of crossover points separately. AFM content: 0 wt% (black), 1 wt%(red), 2 wt%(green), 4 wt% (blue), 8 wt%(cyan), 16 wt% (magenta). d) The gel point of in-house resin with 0, 1, 2, 4, 8 and 16 wt% AFM within 2-HEA/PEGDA$_{250}$ resin under 4.88 m $\frac{W}{cm^2}$ violet light ($\lambda = 405$ nm). e) The gel point of 0, 1, 2, 4, 8, 16 wt% TEGDMA within 2-HEA/PEGDA$_{250}$ resin under 4.88 m $\frac{W}{cm^2}$ violet light ($\lambda = 405$ nm). (For interpretation of the references to colour in this figure legend, the reader is referred to the web version of this article.)

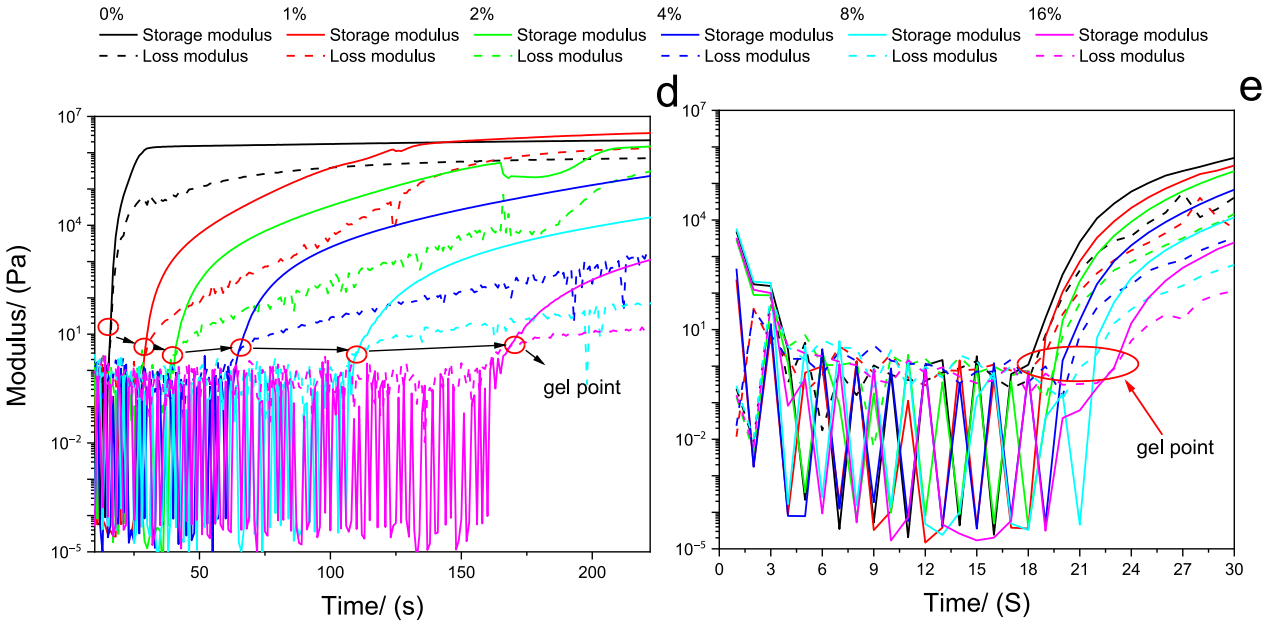

Fig. 11. (*continued*).

Table 3
Gel point formation of 0 wt%, 2 wt% and 4 wt% **3** within 2-HEA/$PEGDA_{250}$ resin at different light intensities.

Light intensity/(L)	Actual/(m $\frac{W}{cm^2}$)	Gel point / (s)		
		0 wt%	**2** wt%	**4** wt%
1	4.88	18	45	73
10	45.0	4	12	23
20	86.3	3	9	15
40	178	2	6	12
60	273	1.8	5	9
80	359	1.5	4.5	7
100	459	1.2	4	5

not macroscopic deformation, and this event occurred more frequently upon increasing [3].

Conversely, the control experiments using TEGDMA as an inactive crosslinker showed an increase in both the instantaneous and cumulative shrinkage stresses at higher concentration of TEGDMA, and the stress evolution was distributed over a much shorter time interval than the AFM equivalence (Fig. 13**b**). The cumulative shrinkage stress increased from 1.24 to 2.18 MPa by adding 16 wt% TEGDMA. The maximum instantaneous shrinkage stress increased from 0.03 MPa to 0.05 MPa and the stress developed within 3 min due to conventional crosslinking in the absence of β-quaternary vinyl group.

3. Conclusions

The addition-fragmentation monomer (AFM, **3**) utilized in photopolymerization-based 3D printer formulations serves as an efficient and useful additive to help reduce the shrinkage stress in 3D printed materials. The time to attain gel point in the networks increased,

Table 4
Crossover points of various proportion of TEGDMA and **3** within 2-HEA/$PEGDA_{250}$ resin under light intensity 1L (4.88 m $\frac{W}{cm^2}$).

Light intensity (4.88 m $\frac{W}{cm^2}$)	Gel point / (s)	
Weight fraction / (wt%)	TEGDMA	AFM-1
16	24	169
8	23	122
4	21	65
2	20	41
1	20	29
0	18	18

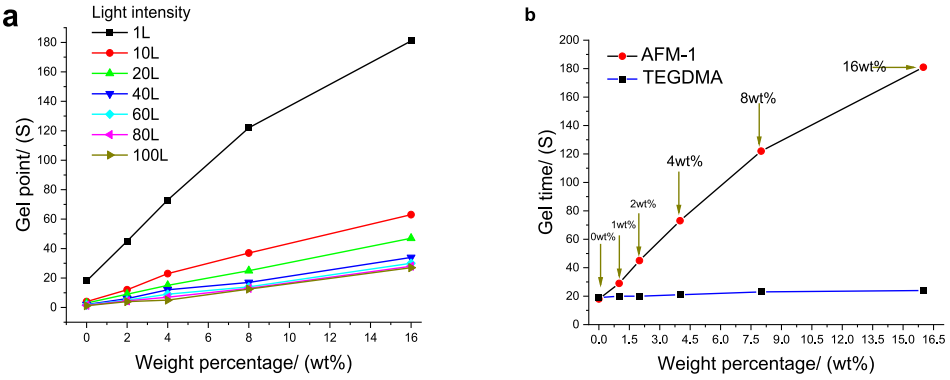

Fig. 12. (a) gel point of 0, 2, 4, 8 and 16 wt% **3** within 2-HEA/$PEGDA_{250}$ resin by varying the light intensity. (b) Gel point under 1L (4.88 m $\frac{W}{cm^2}$) UV light of 0, 1, 2, 4, 8 and 16 wt% TEGDMA and AFM within 2-HEA/$PEGDA_{250}$ resin.

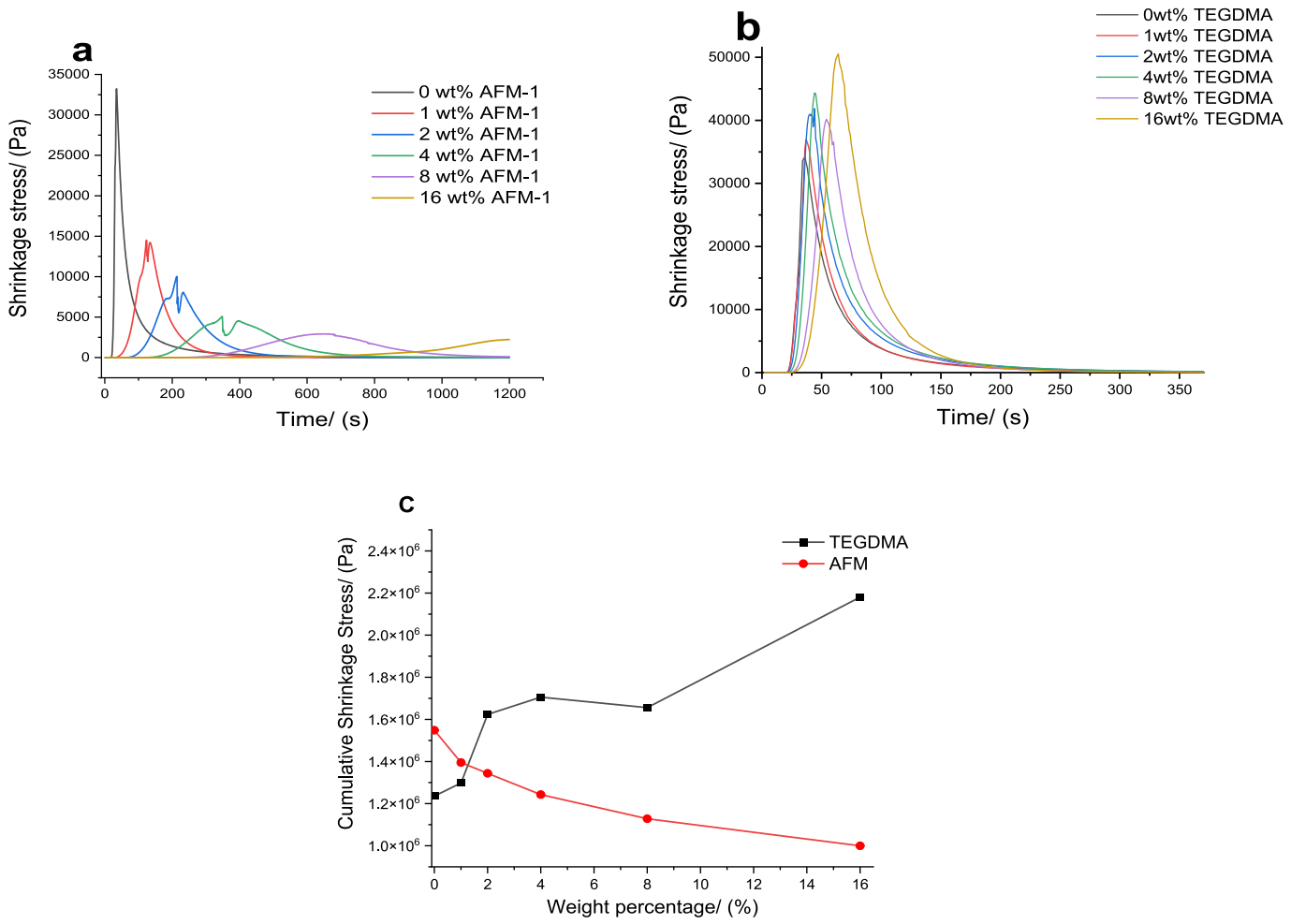

Fig. 13. Calculated shrinkage stress evolution over the curing time of 2-HEA/PEGDA$_{250}$ resin with 0, 1, 2, 4, 8 and 16 wt% a) **3** and b) TEGDMA. c) The cumulative shrinkage stresses of 2-HEA/PEGDA$_{250}$ resin with 0, 1, 2, 4, 8 and 16 wt% **3** and TEGDMA.

conversely, shrinkage stresses were reduced significantly with the introduction of increasing amount of the AFM, as monitored by photorheology and photo FT-IR. The Young's modulus and strength of the printed material with 2-HEA/PEGDA$_{250}$ resin and commercial resins increased with amount of AFM in the formulation. Addition of an AFM results in a reduction in polymerization rate during the 3D printing process, due to the generation of relatively stable substituted methacrylic radical. The reduction of the covalent bond conversion is not obvious at low content of AFM, while the stress relaxation is significant. Thus, small amounts of AFM can enhance strength and diminish the shrinkage stress. The addition-fragmentation monomer shows potential for application in improving the material properties within photolithographic 3D printing. It is also noted that when assessing properties of 3D printed parts, it is important to measure over several days to ensure final properties have stabilized.

CRediT authorship contribution statement

Zhongyuan Wan: Data curation, Formal analysis. **Lee Wai Hin:** Data curation, Formal analysis. **Ataulla Shegiwal:** Methodology, Supervision, Writing – review & editing. **David Haddleton:** Conceptualization, Funding acquisition, Investigation, Project administration, Supervision, Validation, Visualization, Writing – review & editing.

Declaration of Competing Interest

The authors declare that they have no known competing financial interests or personal relationships that could have appeared to influence the work reported in this paper.

Data availability

Data will be made available on request.

Acknowledgements

We thank the Research Technology Platforms (RTP) of the University of Warwick for providing training and equipment and EPSRC for equipment funded in part by EPSRC EP/V036211/1 and EP/V007688/1.

Appendix A. Supplementary material

Supplementary data to this article can be found online at https://doi.org/10.1016/j.eurpolymj.2023.112324.

References

[1] J. Zhang, P. Xiao, 3D printing of photopolymers, Polym. Chem. 9 (13) (2018) 1530–1540, https://doi.org/10.1039/c8py00157j.
[2] M.R. Khosravani, P. Soltani, K. Weinberg, T. Reinicke, Structural integrity of adhesively bonded 3D-printed joints, Polym. Test. 100 (2021), 107262, https://doi.org/10.1016/J. Polymer Testing. 2021.107262.
[3] M. Pizzorni, E. Lertora, A. Parmiggiani, Adhesive bonding of 3D-printed short- and continuous-carbon-fiber composites: an experimental analysis of design methods to

improve joint strength, Compos. Part B Eng. 230 (2022) 109539. 10.1016/J.CompositesB.2021.109539.
[4] E. Saleh, P. Woolliams, B. Clarke, A. Gregory, S. Greedy, C. Smartt, R. Wildman, I. Ashcroft, R. Hague, P. Dickens, C. Tuck, 3D inkjet-printed UV-curable inks for multi-functional electromagnetic applications, Addit. Manuf. 13 (2017) 143–148, https://doi.org/10.1016/j.addma.2016.10.002.
[5] X. Mu, F. Agostinacchio, N. Xiang, Y. Pei, Y. Khan, C. Guo, P. Cebe, A. Motta, D. L. Kaplan, Recent advances in 3D printing with protein-based inks, Prog. Polym. Sci. 115 (2021) 101375.
[6] N. Hossain, M.A. Chowdhury, M.B.A. Shuvho, M.A. Kashem, M. Kchaou, 3D-Printed objects for multipurpose applications, J. Mater. Eng. Perform. 30 (7) (2021) 4756–4767.
[7] R. Marinescu, D. Popescu, D. Laptoiu, A review on 3D-printed templates for precontouring fixation plates in orthopedic surgery, J. Clin. Med. Multidisciplinary Digital Publishing Institute (MDPI) (2020) 1–17. 10.3390/jcm9092908.
[8] H. Gao, G.F.R. Chen, P. Xing, J.W. Choi, H.Y. Low, D.T.H. Tan, High-resolution 3D printed photonic waveguide devices, Adv. Opt. Mater. 8 (18) (2020) 2000613, https://doi.org/10.1002/adom.202000613.
[9] M. Sangermano, A. Chiolerio, G. Marti, P. Martino, UV-cured acrylic conductive inks for microelectronic devices, Macromol. Mater. Eng. 298 (6) (2013) 607–611, https://doi.org/10.1002/MAME.201200072.
[10] M. Shirai, H. Okamura, UV-curable positive photoresists for screen printing plate, Polym. Int. 65 (4) (2016) 362–370, https://doi.org/10.1002/PI.5065.
[11] J.W. Stansbury, M.J. Idacavage, 3D printing with polymers: challenges among expanding options and opportunities, Dent. Mater. 32 (1) (2016) 54–64, https://doi.org/10.1016/J.DENTAL.2015.09.018.
[12] A. Dawood, B.M. Marti, V. Sauret-Jackson, A. Darwood, 3D Printing in Dentistry, Br. Dent. J. 2015 21911 219(11) (2015) 521–529. 10.1038/sj.bdj.2015.914.
[13] A.M.E. Arefin, N.R. Khatri, N. Kulkarni, P.F. Egan, Polymer 3D printing review: materials, process, and design strategies for medical applications, Polymers 13 (9) (2021) 1499, https://doi.org/10.3390/polym13091499.
[14] T.A. Campbell, O.S. Ivanova, 3D printing of multifunctional nanocomposites, Nano Today 8 (2) (2013) 119–120, https://doi.org/10.1016/j.nantod.2012.12.002.
[15] K. Miyamoto, N. Watanabe, Y. Takefuji, Adaptation to other agent's behavior using meta-strategy learning by collision avoidance simulation, Appl. Sci. 11 (4) (2021) 1–14, https://doi.org/10.3390/app11041786.
[16] S.C. Ligon, R. Liska, J. Stampfl, M. Gurr, R. Mülhaupt, Polymers for 3D printing and customized additive manufacturing, Chem. Rev. 117 (15) (2017) 10212–10290, https://doi.org/10.1021/acs.chemrev.7b00074.
[17] C.W. Hull, Apparatus for production of three dimensional objects by stereolithography, 11 March 1986.
[18] C. Sun, N. Fang, D.M. Wu, X. Zhang, Projection micro-stereolithography using digital micro-mirror dynamic mask, Sens. Actuat. A 121 (1) (2005) 113–120, https://doi.org/10.1016/j.sna.2004.12.011.
[19] H. Deng, J. Lin, 4D printing: 3D printing of responsive and programmable materials, in: 3D Bioprinting and Nanotechnology in Tissue Engineering and Regenerative Medicine, Academic Press, 2022, pp 213–237. 10.1016/B978-0-12-824552-1.00012-8.
[20] J. Zhang, Q. Hu, S. Wang, J. Tao, M. Gou, Digital light processing based three-dimensional printing for medical applications, Int. J. Bioprinting 6 (1) (2020) 12–27, https://doi.org/10.18063/ijb.v6i1.242.
[21] J.W. Stansbury, M. Trujillo-Lemon, H. Lu, X. Ding, Y. Lin, J. Ge, Conversion-dependent shrinkage stress and strain in dental resins and composites, Dent. Mater. 21 (2005) 56–67, https://doi.org/10.1016/j.dental.2004.10.006.
[22] X. Shi, J. Zhang, N. Corrigan, C. Boyer, Controlling mechanical properties of 3D printed polymer composites through photoinduced reversible addition-fragmentation chain transfer (RAFT) polymerization, Polym. Chem. 13 (1) (2022) 44–57, https://doi.org/10.1039/d1py01283e.
[23] A. Bagheri, K.E. Engel, C.W.A. Bainbridge, J. Xu, C. Boyer, J. Jin, 3D Printing of polymeric materials based on photo-RAFT polymerization, Polym. Chem. 11 (3) (2020) 641–647, https://doi.org/10.1039/c9py01419e.
[24] Z. Zhang, N. Corrigan, A. Bagheri, J. Jin, C. Boyer, A versatile 3D and 4D printing system through photocontrolled RAFT polymerization, Angew. Chemie - Int. Ed. 58 (50) (2019) 17954–17963, https://doi.org/10.1002/anie.201912608.
[25] A. Bagheri, C.M. Fellows, C. Boyer, Reversible deactivation radical polymerization: from polymer network synthesis to 3D printing, Adv. Sci. 8 (5) (2021) 2003701.
[26] V.A. Bobrin, J. Zhang, N. Corrigan, C. Boyer, X. Shi, J. Zhang, N. Corrigan, C. Boyer, V.A. Bobrin, J. Zhang, N. Corrigan, C. Boyer, A. Bagheri, C.M. Fellows, C. Boyer, The emergence of reversible-deactivation radical polymerization in 3D printing, Adv. Mater. Technol. 8 (5) (2022) 2201054, https://doi.org/10.1002/admt.202201054.
[27] Guy D. Joly, Larry R. Krepski, Anne R. Fornof, Serkan Yurt, Babu N. Gaddam, Ahmed S. Abuelyaman, Michael A. Kropp, Addition-Fragmentation Agents, EP3502092A1, 26 June 2019.
[28] William H. Moser, Ann R. Fornof, Guy D. Joly, Serkan YURT, Larry R. Krepski, Ahmed S. Abuelyaman, Afshin Falsafi, Bradley D. Craig, Joel D. Oxman, B. N. G. Addition-Fragmentation Oligomers. WO2016133668A1, 25 August 2016.
[29] G. Joly, A.S. Abuelyaman, R.S. Davidson, T.D. Jones, B.N. Gaddam, S.J. Moench, Photoinitiated Oligomerizatio of Methacrylate Esters, WO2014116461A1, 31 July 2014.
[30] William H. Moser, Ann R. Fornof, Guy D. Joly, Serkan Yurt, Larry R. Krepski, Ahmed S. Abuelyaman, Afshin Falsafi, Bradley D. Craig, Joel D. Oxman, B.N.G, Addition-Fragmentation Oligomers. US20200031961A1, 30 January 2020.
[31] Ann R. Fornof, William H. Moser, G. D. J. Addition-Fragmentation Oligomers Having High Refractive Index Groups. US20160346170A1, 1 December 2016.
[32] A.R. Fornor, W.H. Moser, L.R. Krepski., G.D. Joly, A.S. Abuelyaman, A. Falsafi, B.N. Gaddam, Addition-Fragmentation Oligomers. US2018044448A1, 15 February 2018.
[33] Ann R. Fornof, William H. Moser, G.D.J., Addition-fragmentation oligomers having high refractive index groups, WO2015126657A1, 27 August 2015.
[34] Ahmed S. Abuelyaman, Babu N. Gaddam, Afshin Falsafi, Tianyu WuYizhong Wang, Randilynn B. Christensen, W. H. M., Addition-fragmentation agent with pendent amine groups, WO2020075007A1, 16 April 2020.
[35] P.K. Shah, J.W. Stansbury, C.N. Bowman, Application of an addition-fragmentation-chain transfer monomer in Di(meth)acrylate network formation to reduce polymerization shrinkage stress, Polym. Chem. 8 (30) (2017) 4339–4351, https://doi.org/10.1039/c7py00702g.
[36] C.J. Kloxin, C.N. Bowman, Covalent adaptable networks: smart, reconfigurable and responsive network systems, Chem. Soc. Rev. 42 (17) (2013) 7161–7173.
[37] L. Leibler, M. Rubinstein, R.H. Colby, Dynamics of reversible networks, Macromolecules 24 (16) (1991) 4701–4707, https://doi.org/10.1021/ma00016a034.
[38] J.C. Kloxin, F.T. Scott, N.C. Bowman, Stress relaxation via addition fragmentation chain transfer in a thiol-ene photopolymerization, Macromolecules 42 (7) (2009) 2551–2556, https://doi.org/10.1021/ma802771b.
[39] H.Y. Park, C.J. Kloxin, T.F. Scott, C.N. Bowman, Covalent adaptable networks as dental restorative resins: stress relaxation by addition-fragmentation chain transfer in allyl sulfide-containing resins, Dent. Mater. 26 (10) (2010) 1010–1016, https://doi.org/10.1016/j.dental.2010.06.007.
[40] D.M. Haddleton, D.R. Maloney, K.G. Suddaby, A. Clarke, S.N. Richards, Radical-addition-fragmentation and co-polymerization of methyl methacrylate macromonomers from catalytic chain transfer polymerization (CCTP), Polymer 38 (25) (1997) 6207–6217, https://doi.org/10.1016/S0032-3861(97)00180-8.
[41] D.M. Haddleton, D.R. Maloney, K.G. Suddaby, Competition between β-scission of macromonomer-ended radicals and chain transfer to cobalt(II) in catalytic chain transfer polymerization (CCTP), Macromolecules 29 (1) (1996) 481–483, https://doi.org/10.1021/MA9507756.
[42] G. Nurumbetov, N. Engelis, J. Godfrey, R. Hand, A. Anastasaki, A. Simula, V. Nikolaou, D.M. Haddleton, Methacrylic block copolymers by sulfur free RAFT (SF RAFT) free radical emulsion polymerisation, Polym. Chem. 8 (6) (2017) 1084–1094, https://doi.org/10.1039/C6PY02038K.
[43] G. Moad, E. Rizzardo, S.H. Thang, Radical addition-fragmentation chemistry in polymer synthesis, Polymer 49 (5) (2008) 1079–1131, https://doi.org/10.1016/J.POLYMER.2007.11.020.
[44] Y.K. Chong, G. Moad, E. Rizzardo, S.H. Thang, Thiocarbonylthio end group removal from RAFT-synthesized polymers by radical-induced reduction, Macromolecules 40 (13) (2007) 4446–4455, https://doi.org/10.1021/ma062919u.
[45] J. Chiefari, Y.K. Chong, F. Ercole, J. Krstina, J. Jeffery, T.P.T. Le, R.T. A. Mayadunne, G.F. Meijs, C.L. Moad, G. Moad, E. Rizzardo, S.H. Thang, Living free-radical polymerization by reversible addition - fragmentation chain transfer: the RAFT process, Macromolecules 31 (16) (1998) 5559–5562, https://doi.org/10.1021/ma9804951.
[46] M. Chen, G. Moad, E. Rizzardo, Thiocarbonylthio end group removal from RAFT-synthesized polymers by a radical-induced process, J. Polym. Sci. Part A Polym. Chem. 47 (23) (2009) 6704–6714, https://doi.org/10.1002/pola.23711.
[47] C.J. Kloxin, T.F. Scott, B.J. Adzima, C.N. Bowman, Covalent adaptable networks (CANs): a unique paradigm in cross-linked polymers, Macromolecules 43 (6) (2010) 2643–2653, https://doi.org/10.1021/ma902596s.
[48] C.N. Bowman, C.J. Kloxin, Covalent adaptable networks: reversible bond structures incorporated in polymer networks, Angew. Chemie Int. Ed. 51 (18) (2012) 4272–4274, https://doi.org/10.1002/ANIE.201200708.
[49] G.D. Joly, L.R. Krepski, B.N. Gaddam, A.S. Abuelyaman, B.D. Craig, T.D. Dunbar, C. Cao, J.D. Oxman, A. Falsafi, W.H. Moser, H.T. Bui, Dental compositions comprising ethylenically unsaturated addition-fragmentation agent. EP2965742B1, 8 February 2012.
[50] J.G. Kloosterboer, G.F.C.M. Lijten, H.M.J. Boots, Network formation by chain crosslinking photopolymerization and some applications in electronics, Makromol. Chemie. Macromol. Symp. 24 (1) (1989) 223–230, https://doi.org/10.1002/MASY.19890240123.
[51] A. Mautner, X. Qin, H. Wutzel, S.C. Ligon, B. Kapeller, D. Moser, G. Russmueller, J. Stampfl, R. Liska, Thiol-ene photopolymerization for efficient curing of vinyl esters, J. Polym. Sci. Part A Polym. Chem. 51 (1) (2013) 203–212, https://doi.org/10.1002/POLA.26365.
[52] C. Gorsche, R. Harikrishna, S. Baudis, P. Knaack, B. Husar, J. Laeuger, H. Hoffmann, R. Liska, Real time-NIR/MIR-photorheology: a versatile tool for the in situ characterization of photopolymerization reactions, Anal. Chem. 89 (9) (2017) 4958–4968, https://doi.org/10.1021/acs.analchem.7b00272.
[53] H.H. Winter, Can the gel point of a cross-linking polymer be detected by the G′ – G″ crossover? Polym. Eng. Sci. 27 (22) (1987) 1698–1702, https://doi.org/10.1002/PEN.760272209.
[54] H.H. Winter, F. Chambon, Analysis of linear viscoelasticity of a crosslinking polymer at the gel point, J. Rheol. 30 (2) (1986) 367–382, https://doi.org/10.1122/1.549853.
[55] H. Murata, Rheology - theory and application to biomaterials, PolymerizationIntechOpen (2012) 403–426, https://doi.org/10.5772/48393.
[56] C. Walling, Gel formation in addition polymerization, J. Am. Chem. Soc. 67 (3) (1945) 441–447, https://doi.org/10.1021/ja01219a026.
[57] W.H. Li, A.E. Hamielec, C.M. Crowe, Kinetics of the free-radical copolymerization of methyl methacrylate/ethylene glycol dimethacrylate: 2. analysis of gelation and

the pregel region, Polymer 30 (8) (1989) 1518–1523, https://doi.org/10.1016/0032-3861(89)90226-7.
[58] G.D. Joly, L.R. Krepski, B.N. Gaddam, A.S. Abuelyaman, B.D. Craig, T.D. Dunbar, C. Cao, J.D. Oxman, A. Falsafi, W.H. Moser, H.T. Bui, Dental compositions comprising ethylenically unsaturated addition-fragmentation agent, 16 June 2015.
[59] G.M. Carlson, N. Olmsted, Synthesis of 2,2-dimethyl-4-methyleneglutaric acid and dervatives. US4547323A, 15 October 1985.